RESEARCH ARTICLE

Quantification of lung surfactant lipid (dipalmitoylphosphatidylcholine/sphingomyelin) ratio in binary liposomes using Raman spectroscopy

Aneesh Vincent Veluthandath[1] | Waseem Ahmed[1] | Jens Madsen[2] |
Howard W. Clark[2] | Anthony D. Postle[3] | James S. Wilkinson[1] |
Ganapathy Senthil Murugan[1]

[1]Optoelectronics Research Centre, University of Southampton, Southampton, UK

[2]Neonatology, EGA Institute for Women's Health, Faculty of Population Health Sciences, University College London, London, UK

[3]Academic Unit of Clinical & Experimental Sciences, Faculty of Medicine, University of Southampton, Southampton, UK

Correspondence

Aneesh Vincent Veluthandath and Ganapathy Senthil Murugan, Optoelectronics Research Centre, University of Southampton, Southampton SO17 1BJ, UK.
Email: avv1a15@soton.ac.uk and smg@orc.soton.ac.uk

Abstract

Early diagnosis of neonatal respiratory distress syndrome (nRDS) is important in reducing the mortality of preterm babies. Knowledge of the ratio of two components of lung surfactant, dipalmitoylphosphatidylcholine (DPPC), and sphingomyelin (SM) can be used as biomarkers of lung maturity and inform treatment. Raman spectroscopy is a powerful tool to analyze vibrational spectra of organic molecules which requires only limited sample preparation steps and, unlike IR spectroscopy, is not masked by water absorption. In this paper, we explore the potential of using Raman spectroscopy as a tool to estimate the ratio of DPPC and SM from aqueous vesicles of binary mixture of DPPC and SM. We demonstrate that the ratio of DPPC and SM can be estimated by estimating the ratio of intensity of C=O stretch of DPPC and C=C stretch of SM as well as C=O stretch of DPPC and amide I of SM. Further, we employ a partial least squares regression (PLSR) model to automate the estimation and demonstrate that PLSR method can predict the DPPC and SM ratio with an R^2 value of 0.968.

KEYWORDS

lipid vesicles, liposome, machine learning, neonatal respiratory distress syndrome, phospholipids, Raman spectroscopy

1 | INTRODUCTION

Lipids, especially phospholipids, are the building blocks of the lipid bilayer that forms the cell plasma membrane and membranes of intracellular vesicles.[1] Phospholipids consists of a hydrophilic phosphate containing headgroup and one or two hydrophobic fatty acid chains.[1] The phosphate in the headgroup is typically connected to an alcohol such as choline, inositol, glycerol or to a carbohydrate[2] The phosphate headgroup is attached to the

fatty acid chain through a backbone molecule, with glycerol and sphingosine being the most common.[2] In the presence of water, phospholipids arrange themselves into lipid bilayers and vesicles which can act as barriers to water but which are transparent to small molecules such as oxygen and carbon dioxide.

Phosphatidylcholine (PC)—also known as lecithin—is a major component of mammalian cell membranes, comprising two fatty acyl chains attached to a glycerophosphocholine backbone by ester bonds. PC comprises many individual molecular species defined by the combination of fatty acyl chains. Dipalmitoylphosphatidylcholine (DPPC) is the most abundant PC species, with two esterified saturated palmitoyl acyl chains.[1] DPPC has been widely used to prepare lipid bilayer model membranes in research,[3] by either the Langmuir–Blodgett[4] or liposome methods.[5] Sphingomyelin (SM) is another significant component of mammalian cell membranes[6] comprising a sphingosine backbone with one esterified fatty acid, typically palmitate. SM confers rigidity to the cell membranes due to its ability to form hydrogen bonds using the hydrogen donating amide and hydroxyl moieties present in the sphingosine backbone and hydrogen accepting moieties of headgroup and fatty acid chain.[7] Together with cholesterol, SM forms specialized domains in cell membranes called lipid rafts. Lipid rafts are detergent resistant; therefore, these can be isolated from cell membranes using a non-ionic detergent such as Triton X-100. Lipid rafts are important in targeted binding and immune signaling.[6]

Liposomes are small artificial vesicles made from amphiphilic lipids, such as PC and SM. They can be used as model systems[8] to study cell membrane dynamics in the laboratory. Several experimental techniques such as differential scanning calorimetry,[9] fluorescent imaging,[10] atomic force microscopy, and Raman imaging are used to study liposomes to understand the domain separation, domain co-existence, lateral separation, and phase transition in biological membranes. Liposomes are also used in targeted drug delivery, gene therapy, and vaccines[11] — such as covid-19 mRNA vaccines[12] — due to their biocompatibility, biodegradability and hydrophilic and hydrophobic drug loading capability.[13,14]

Lung surfactant is a complex mixture of lipids and protein that regulates the surface tension of the inner lining of the alveoli and small airways.[15,16] Lungs surfactant reduces the surface tension at the alveolar surface, preventing its collapse during exhalation.[17] Lung surfactant consist of 90% lipids and 10% protein, with DPPC being the major lipid component.[18] Other lipids such as phosphatidylglycerol, phosphatidylinositol, and cholesterol are also present in lung surfactant, with SM being a minor component.[18] Lung surfactant also protects against pathogens and plays a role in the immune response.[19]

Neonatal respiratory distress syndrome (nRDS) is the primary cause of hospitalization, respiratory failure, and death in very preterm neonates.[20] Surfactant deficiency in immature lungs is the principal cause of nRDS and administration of animal derived surfactant therapy at birth has significantly improved survival and disease severity of these very vulnerable infants. Nevertheless, surfactant administration can be detrimental if it is not required when lungs are sufficiently mature. Early detection of nRDS would significantly inform the clinical decision whether to treat with surfactant. Historically, estimation of the ratio of PC (lecithin) to SM (L/S ratio) in amniotic fluid before birth was used to predict nRDS,[21] but the methods used—thin layer chromatography and mass spectrometry—were too time-consuming and laborious to be clinically useful for the rapid decisions required at birth.[21] More recently, Fourier transform infrared spectroscopy (FTIR) was suggested as a more rapid method to diagnose nRDS.[22,23] However, presence of water can mask the fingerprint region of FTIR spectrum and therefore FTIR spectroscopy requires liquid–liquid extraction methods to dissolve lipids in an organic solvent.

Raman spectroscopy is a reliable tool to explore the properties of lipids[24] especially in the case of ratiometric analysis.[25] Compared with chromatography, Raman spectroscopy does not require elaborate sample preparation or labeling. Raman spectroscopy can be used to accurately determine the chain length of organic molecules, functional groups, and degree of unsaturation, which in turn can be used to identify the individual components of a complex mixture.[25] Raman spectroscopy has also been used to investigate the liposome domain formation[26] and phase transitions.[27] Raman spectroscopy requires minimal sample preparation and unlike infrared spectroscopy; the Raman spectrum can be obtained from aqueous solutions.

In this paper, we explore the possibility of detecting nRDS using Raman spectroscopy using synthetic aqueous samples as a model of lung surfactant. We prepared DPPC/SM vesicles as a model system for gastric aspirate extracted from newborn babies. We have prepared aqueous lipid vesicles with DPPC/SM ratio ranging from 0.25 to 3.25 to emulate the lipid concentration around the critical L/S ratio of 2. Raman spectroscopy of samples shows that the L/S ratio can be calculated using ratiometric analysis. Further, we have implemented a partial least squares regression (PLSR) to model and predict the L/S ratio in the vesicles. The model shows high accuracy with R^2 of 0.968. This demonstrates that using Raman spectroscopy, one could potentially diagnose nRDS from gastric aspirate with minimal sample preparation steps. Raman spectroscopy combined with machine learning techniques provides the opportunity for rapid bedside diagnosis.

2 | MATERIALS AND METHODS

2.1 | Materials

We obtained the *N*-palmitoyl-D-erythro-sphingosylphosphorylcholine (16:0 SM) and as a model for lecithin 1,2-dihexadecanoyl-sn-glycero-3-phosphocholine (DPPC/16:0 PC) from Avanti polar lipids. HPLC grade dichloromethane (DCM) was purchased from Sigma Aldrich.

2.2 | Preparation of liposomes

To prepare the 2 mM SM stock solution, 14.06 mg of SM (molar mass 703.028 g) was dissolved in 10 mL of DCM. Two millimolars of DPPC stock solution was prepared by dissolving 14.68 mg of DPPC (molar mass 734.039 g) in DCM. Appropriate amounts of SM and DPPC were aliquoted into glass vials to prepare lipid mixtures. The total lipid contents in the final mixture were maintained as 1 mM. The mixtures were sonicated for 1 min, and then, solvent was allowed to evaporate under nitrogen flow. One milliliter of deionized water was added to the dried films. The glass vials were warmed up to 60°C and vigorously shaken until the solution became turbid. The lipid solutions were transferred to a centrifuge tube and centrifuged at 16,000 g for 25 min. The supernatant, which contains smaller vesicles, was transferred to another glass bottle. The precipitated multilamellar vesicles were pipetted to a Si substrate for further study. Figure 1A–D shows the schematic of sample preparation. A total of 15 samples were prepared, which included 13 samples of vesicles with L/S ratios ranging from 0.25 to 3.25 at intervals of 0.25, as well as vesicles of DPPC and SM. 10 spectra were collected from each sample. The liposomes are pipetted to a Si substrate for imaging and spectroscopy (Figure 1E). A dark field image of vesicles prepared using this method is shown in Figure 1F.

2.3 | Raman spectroscopy

Raman spectroscopy of the samples was carried out using a Renishaw inVia micro-Raman spectrometer with laser excitation at a wavelength of 532 nm. The microscope was set up in epi-florescence configuration. The samples were excited through a 50× objective lens, and the Raman scattered light was collected through the same objective lens. A notch filter was used to filter the excitation laser light from the Raman spectrum. To record the spectra, 25 μL of sample was deposited on a Si wafer. Raman scattering from the Si wafer was used to calibrate the spectrometer. All spectra were recorded at 10 s exposure, with five spectra averaging and the laser power was typically 5 mW. All spectra were recorded at room temperature.

3 | RAMAN SPECTRA OF DPPC AND SM

Figure 2 shows the chemical structure of the (A) DPPC and (B) SM used in the study. Both DPPC and SM are phospholipids. Phospholipids are lipids where a phosphate group is attached to a backbone molecule and one or two fatty acids are attached to the backbone molecule. In the present case, a choline molecule was attached to the phosphate group. A glycerol molecule acts as the

FIGURE 1 (A–D) Work flow of preparation of lipid vesicles. (A) Appropriate amount of DPPC and SM solutions are mixed in a vortex mixer. (B) The mixture was dried under nitrogen flow. (C) DI water was added to the dried film and warmed to 60°C and vortex mixed. (D) The mixture was transferred to a test tube and centrifuged. (E) Precipitate pipetted to a Si substrate for imaging and spectroscopy. (F) Microscope image of DPPC/SM lipid vesicles.
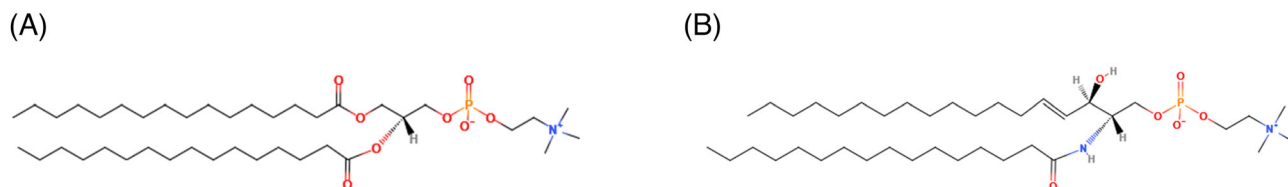
(A)

(B)
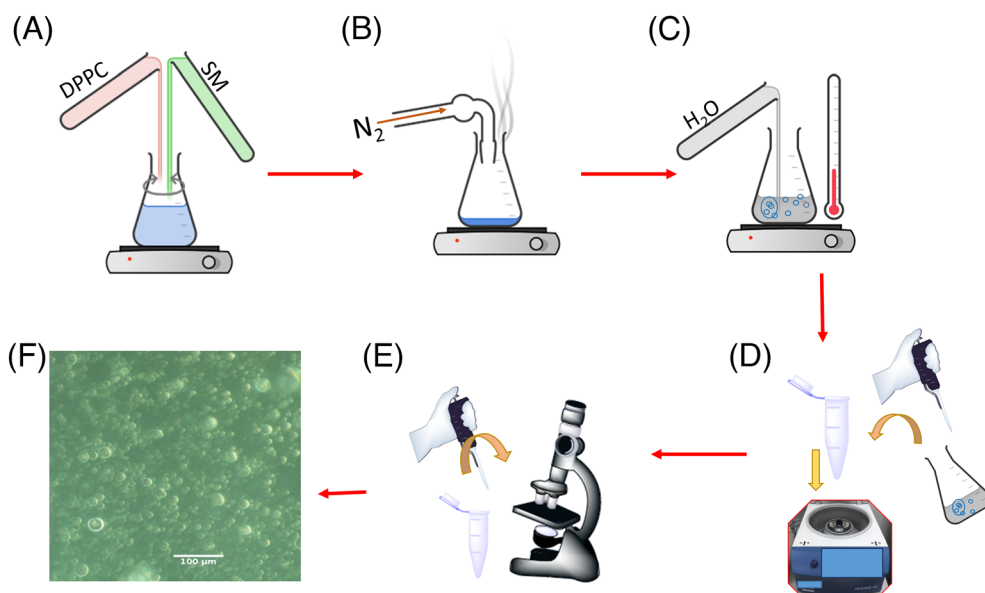
FIGURE 2 Chemical structure of (A) DPPC and (B) SM.
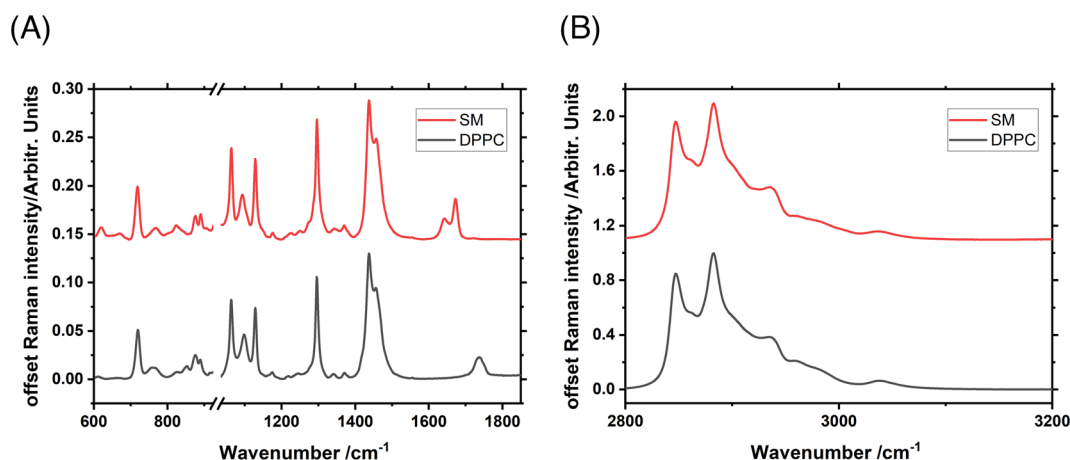
(A)

(B)

FIGURE 3 Raman spectra of DPPC and SM liposomes recorded in (A) the 600–1800 cm^{-1} band and (B) the 2800–3200 cm^{-1} band.

backbone of the DPPC. Two palmitic acid chains are also attached to the glycerol. The backbone molecule of the SM is sphingosine. A palmitic acid chain was attached to sphingosine as the fatty acid chain.

Figure 3A shows the Raman spectra of DPPC and SM recorded in the 600–1800 cm^{-1} region where it shows the vibrations of functional groups. The difference in Raman spectra due to the presence of different molecular conformation can also be observed in this region. DPPC and SM show similar spectra at wavenumbers between 600 and 1600 cm^{-1}. The C—N stretch of the phosphocholine head group is observed at 718.8 cm^{-1} in SM and 720 cm^{-1} for DPPC.[28] A coincident band of gauche C—C stretch and choline head group deformation band was observed at 876 cm^{-1}.[28,29] The trans C—C stretch is observed at 890 cm^{-1}.[29] The C—C stretching region (1000–1200 cm^{-1}) shows both the trans and gauche conformers. The out of phase trans conformers of both SM and DPPC was observed at 1063 cm^{-1}. The in-phase component was observed at 1129 cm^{-1}. The gauche conformers transition of SM was observed at 1093 cm^{-1} and that of DPPC at 1098 cm^{-1}. CH$_2$ twist peak was observed at 1296 cm^{-1}. The width of the CH$_2$ twist peak of SM is slightly higher compared DPPC liposome, confirming that the gauche conformation is higher in SM. The CH$_2$ methylene bend peak of SM and DPPC was observed at 1436 cm^{-1}. An asymmetric methyl band was observed as a shoulder of the methylene bend peaks.

The 1600–1850 cm^{-1} region shows significant differences in the spectrum of DPPC and SM. The C═O stretching vibration was observed in DPPC at 1737 cm^{-1}.[30] The C═C stretching of SM was observed at 1672.7 cm^{-1}.[24] The amide I band of SM was observed at 1641.4 cm^{-1}. The amide I peak appears as a shoulder of the C═C stretch of SM. The amide I band was formed due to the coupling of C═O stretch to an N—H bending vibration.[31] The amide I band is an indication of the structural rigidity of the lipid bilayer.

Figure 3B shows the C—H stretching vibrations of SM and DPPC. The asymmetric C—H methylene stretching was observed at 2847 cm^{-1}, and the symmetric methylene stretching was observed at 2842.8 cm^{-1}. The symmetric C—H terminal methyl stretch was observed at 2936.7 cm^{-1}. The vibrational bands of SM and DPPC are given in Table 1.

4 | RATIOMETRIC ANALYSIS OF DPPC/SM LIPOSOMES

To understand the interaction of DPPC and SM in lipid vesicles, vesicles containing different ratios of DPPC and SM were prepared as described in Section 2. Raman spectra of the vesicles in the fingerprint region (600–1600 cm^{-1}) are shown in Figure 4A. The lipid vesicles show similar spectra in the 600–1600 cm^{-1} range. The

region containing the amide I band and the C=C stretch of SM and C=O stretch of DPPC is shown in Figure 4B. Spectra are vertically offset for clarity. The C=O stretch of the carbonyl bond of the DPPC occurs at 1742 cm^{-1} and unique to DPPC and therefore can be used as a measure of the total DPPC present in the sample. In the molecules, only SM has a carbon double bond, and it is relatively immune to the influence of DPPC. SM also shows amide I vibrations. Therefore, the C=C stretching vibration and amide I band can be used as a measure of total SM contained in the mixture.

Figure 5A shows the 1600 to 1800 cm^{-1} region of spectra normalized to the C=C stretch of SM for various L/S ratios. SM is capable of forming intermolecular hydrogen bonds involving 2NH atoms resulting in stiffer lipid bilayer[7] whereas DPPC is usually of forms hydrogen bonds using the head group. The decrease in the amplitude of the amide bond vibration indicates the weakening of intermolecular interaction between SM molecules due to the intercalation of DPPC.

The ratio of the Raman intensities resulting from the C=O stretch of DPPC and the C=C stretch of SM is shown Figure 5B, where it can be seen that the ratio increases with increase in DPPC concentration. Similar trends were also observed by Shirota et al.[26] The linear fit of the data point is also shown in Figure 5B. The linear fit has a slope of 0.79 ± 0.06. The linear fit has an R^2 value of 0.97. The ratio of C=O stretch and amide I band also increases with increase in DPPC concentration, albeit nonlinearly. Figure 5B also shows a second-order polynomial fit ($R^2 = 0.98$) to the $I_{C=O}/I_{Amide\ I}$ ratio. These curves can be used to estimate the ratio of DPPC and SM in an unknown sample. The heterogeneity of samples
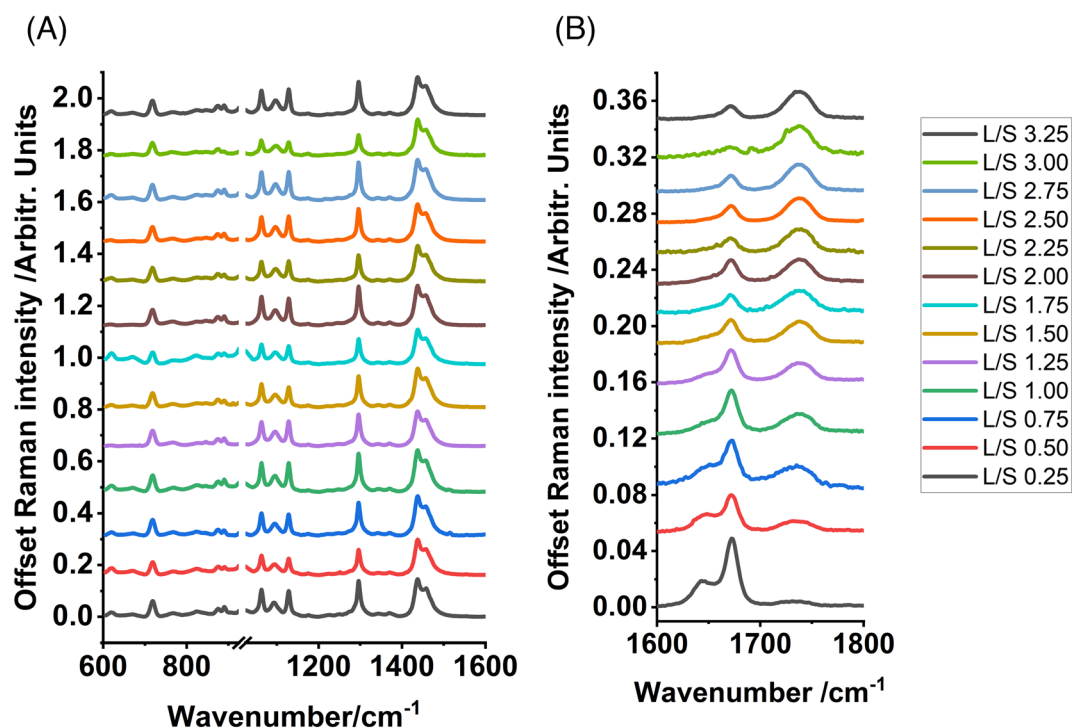
TABLE 1 Assignment of Raman peaks of DPPC and SM.

Raman shift (cm^{-1})	Assignment
718–720	C—N stretch
876	Gauche acyl C—C stretching + choline deformation
890	acyl C—C stretching (trans)
953	CN asymmetric stretching
1062	C—C stretching (trans)
1092–1097	C—C stretching (gauche)
1128	C—C stretching (trans)
1296	CH$_2$ twist
1436–1440	CH$_2$ deformation
1641	Amide I band
1672	C=C stretch
1737	C=O stretching
2846	Asymmetric C—H methylene stretch
2881	symmetric C—H methylene stretch
2933	C—H terminal methyl stretching

FIGURE 4 Raman spectra of DPPC/SM vesicle in the 600–1600 cm^{-1} (A) with different L/S ratio. Spectra are offset for clarity. Raman spectra of vesicles in 1600–1800 cm^{-1} showing amide I band, C=C stretch, and C=O vibrations are shown in (B).
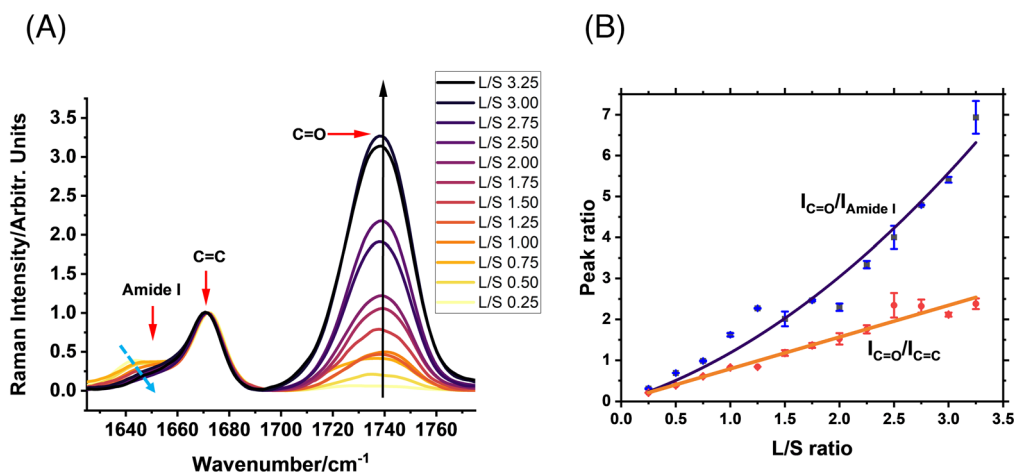
(A)

(B)

FIGURE 5 (A) 1600 to 1800 cm^{-1} region of spectra normalized to C=C stretch of SM. (B) Ratio of C=O stretch of DPPC and C=C stretch of SM and C=O stretch and amide I band as a function of L/S ratio. The error bar shows standard deviation from measurements at various locations of the same sample.

was investigated by acquiring the spectra at different locations in the samples. The spectral intensity showed variation as high as 50% from the average peak intensities across sample position. This is because of the size and distribution difference of the vesicles. However, the observed variation is comparable among amide I, C=C stretch, and C=O stretch indicating a homogeneous distribution of DPPC and SM across different vesicles. The normalized spectra show much lower deviation. The observed inhomogeneity in estimation of L/S ratio is plotted as error bars in Figure 5B. We have observed that the variation in amide I band is higher compared with C=C stretch. This could be because the amide I band is sensitive to the hydration state of the sample. Accuracy of these curves can be increased by acquiring large set of data and employing machine learning algorithms. The reported values of the concentration of lipids in lung aspirates were 0.12–0.6 μmol/mL.[22] Because we used a centrifugation step in our sample preparation, it is difficult to predict the actual concentration of lipids in the measured sample. To establish that Raman spectroscopy can be useful on samples with physiologically relevant concentration, we have prepared samples with concentration 10, 1, 0.5, 0.1, and 0.01 μmol/mL 1 mL aqueous solution. The centrifugation step was omitted to maintain the total lipids concentration in the sample. Fifty microliters of sample was pipetted to a Si wafer, and Raman spectra were recorded (see Figure S1). The exposure time was 40 s and averaged over four spectra. We were able to observe Raman spectra with a lipid concentration 1 order of magnitude lower (0.01 μmol/mL) than physiologically relevant concentrations (0.12–0.6 μmol/mL) which demonstrates that Raman can be used to measure L/S in physiologically relevant concentrations.

One of the important parameters to consider when detecting chemicals using Raman spectroscopy is the limit of detection (LOD). To detect analytes using Raman spectroscopy, the Raman Intensity needs to be two to three times greater than the intensity of the noise background.[32] To determine the LOD, we prepared lipid vesicles with total lipid concentration of 10, 1, 0.5, 0.1, and 0.01 mM and recorded spectra. For LOD determination, we used the expression $I_{Raman} > 2 \times \sqrt{I_{Raman} + I_{Background}}$, where I_{Raman} is Raman intensity and $I_{Background}$ is the background intensity.[32] A concentration of 0.01 mM was sufficient to detect spectra using C=C stretching and C=O stretching, while amide I required a slightly higher concentration of 0.1 mM (see Figure S2). However, it is important to note that the intensity of Raman spectra varies considerably in each sample due to differences in vesicle size and distribution. To account for this variability, we also estimated the LOD using the calibration curve. The LOD is defined as[33]

$$LOD = \frac{2\sqrt{2}\,\sigma}{\rho},$$

where σ is the standard deviation of the background signal estimated using a blank sample and ρ is the slope of calibration curve. The estimated value of σ was 92.81, and the slopes from the calibration curve were 933.57 for the amide I peak, 2575.40 for C=C stretch, and 5755.74 for C=O stretch (see Figure S3). Using the expression mentioned above, the LOD for the amide I bond was 0.28 mM; for C=C stretching, it was 0.1 mM; and for C=O stretching, it was 0.04 mM. The C=O stretching mode of DPPC has lower detection limit compared with Raman vibrations of SM; therefore, the LOD is limited by
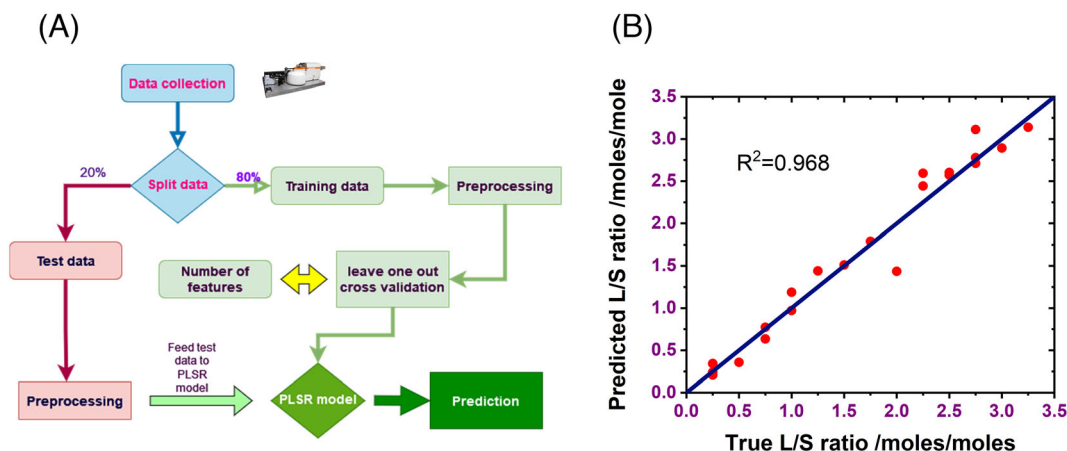
FIGURE 6 (A) Workflow of machine learning method used in the study. Correlation plot of true and predicted L/S ratio of test set samples is shown in (B).

the detection limit of amide I mode and C=C stretching mode, and we can infer that the LOD in ratiometric analysis is 0.28 mM using amide I bond and C=O stretching and 0.1 mM using C=C vibrations and C=O stretching. The LOD can be improved by improving the signal-to-noise ratio.

5 | PLSR OF RAMAN SPECTRA

Machine learning methods are recently gaining popularity in the analysis of Raman spectra because of their prediction accuracy and ability to analyze large sets of data.[34] We have used PLSR, a supervised multivariate method, to analyze and predict the L/S ratio. We chose PLSR because it addresses issues related to multicollinearity in spectral data and allows us to develop robust prediction models.[22] Raman spectra were baseline corrected using Spectrogryph software,[35] and the PLSR analysis was performed using the quant module of Operant LLC, Peak® spectroscopy software. Figure 6A shows the work flow used in the machine learning methods. All spectra were vector normalized before analysis. The spectra were split into 80:20 ratios as train and test sets. This approach was chosen because it avoids a "data leakage" scenario where information in the test dataset is inadvertently used to improve the performance of the PLSR model. By separating these two datasets before any pre-processing, all enhancements to the model's performance are solely based on the information available in the training dataset, making the prediction outputs from the test dataset more likely to reflect real-world performance. The PLSR model was trained using the train dataset and optimized using leave-one-out cross-validation. Figure 6B shows the prediction results of L/S ratio of the test set, for which the R^2 of the prediction was 0.968. Collecting

additional data would increase confidence in the broader applicability, generalizability, and performance of this approach for predicting the L/S ratio. However, the primary purpose of this study was to explore whether it is possible to use Raman spectroscopy for determining the L/S ratio, as has been demonstrated.

6 | CONCLUSIONS

Raman spectroscopy is a powerful and versatile technique to potentially quantify the constituents of bio-membranes. Raman spectroscopy can be carried out in aqueous environment and requires very little sample preparation. DPPC and SM are two important constituents of bio-membranes and also participate in cell signaling and formation of lipid rafts. Knowing the ratio of DPPC and SM in lung surfactant of preterm babies is important when evaluating the lung maturity and could in the future be an important consideration when deciding the course of action of critical care. In this paper, we have used aqueous vesicles of DPPC and SM as a model of lung surfactant. We demonstrated that the L/S ratio can be measured from aqueous vesicles using Raman spectroscopy, demonstrating potential for rapid bedside diagnosis of nRDS. The Raman intensity ratios $I_{C=O}/I_{C=C}$ and $I_{C=O}/I_{Amide\,I}$ are proportional to the L/S ratio. We have also observed weakening amide I Raman vibration of SM due to the weakening of intramolecular hydrogen bond between SM molecules with addition of DPPC. We propose that the L/S ratio of an unknown sample can be deduced from $I_{C=O}/I_{C=C}$ and $I_{C=O}/I_{Amide\,I}$. We further demonstrated that a PLS regression model can predict the L/S ratio in vesicles with high accuracy. Further studies using complex mixtures and clinical samples will be carried out in the future.

AUTHOR CONTRIBUTIONS

ACKNOWLEDGMENTS

CONFLICT OF INTEREST STATEMENT

The authors declare no conflict of interest.

DATA AVAILABILITY STATEMENT

Data supporting this study are available from the University of Southampton repository at: https://doi.org/10.5258/SOTON/D2521

REFERENCES

[1] T. Harayama, H. Riezman, *Nat. Rev. Mol. Cell Biol.* **2018**, *19*, 281.

[2] B. Alberts, A. Johnson, J. Lewis, M. Raff, K. Roberts, P. Walter, *Molecular Biology of the Cell*, 4th ed., Garland Science, New York **2002**.

[3] M. Khvedelidze, T. Mdzinarashvili, E. Shekiladze, M. Schneider, D. Moersdorf, I. Bernhardt, *J. Liposome Res.* **2015**, *25*, 20.

[4] H. A. Rinia, R. A. Demel, J. P. J. M. Van Der Eerden, B. De Kruijff, *Biophys. J.* **1999**, *77*, 1683.

[5] S. J. Attwood, Y. Choi, Z. Leonenko, *Int. J. Mol. Sci.* **2013**, *14*, 3514.

[6] L. Rajendran, K. Simons, *J. Cell Sci.* **2005**, *118*, 1099.

[7] J. P. Slotte, *Biochim. Biophys. Acta, Biomembr.* **2016**, *1858*, 304.

[8] A. Tukova, A. Rodger, *Emerg. Top Life Sci.* **2021**, *5*, 61.

[9] P. R. Maulik, G. G. Shipley, *Biochemistry* **1996**, *35*, 8025.

[10] S. L. Veatch, S. L. Keller, *Biophys. J.* **2003**, *85*, 3074.

[11] N. Pardi, M. J. Hogan, F. W. Porter, D. Weissman, *Nat. Rev. Drug Discov.* **2018**, *17*, 261.

[12] N. Chaudhary, D. Weissman, K. A. Whitehead, *Nat. Rev. Drug Discov.* **2021**, *20*, 817.

[13] P. Nakhaei, R. Margiana, D. O. Bokov, W. K. Abdelbasset, M. A. Jadidi Kouhbanani, R. S. Varma, F. Marofi, M. Jarahian, N. Beheshtkhoo, *Front. Bioeng. Biotechnol.* **2021**, *9*, 1.

[14] P. Walde, S. Ichikawa, *Appl. Sci.* **2021**, *11*, 10345. https://doi.org/10.3390/app112110345

[15] R. Veldhuizen, K. Nag, S. Orgeig, F. Possmayer, *Biophys. Acta - Mol. Basis Dis.* **1998**, *1408*, 90.

[16] C. B. Daniels, S. Orgeig, *News Physiol. Sci.* **2003**, *18*, 151.

[17] J. C. Jackson, *in Avery's Diseases of the Newborn*, 9th ed., Elsevier, Philadelphia **2012** 633.

[18] P. O. Nkadi, T. A. Merritt, D. A. M. Pillers, *Mol. Genet. Metab.* **2009**, *97*, 95.

[19] S. H. Han, R. K. Mallampalli, *Ann. Am. Thorac. Soc.* **2015**, *12*, 765.

[20] P. Stylianou-Riga, T. Boutsikou, P. Kouis, P. Kinni, M. Krokou, A. Ioannou, T. Siahanidou, Z. Iliodromiti, T. Papadouri, P. K. Yiallouros, N. Iacovidou, *Ital. J. Pediatr.* **2021**, *47*, 1.

[21] C. Autilio, *Biomed. J.* **2021**, *44*, 671.

[22] W. Ahmed, A. V. Veluthandath, D. J. Rowe, J. Madsen, H. W. Clark, A. D. Postle, J. S. Wilkinson, G. S. Murugan, *Sensors* **2022**, *22*, 1744.

[23] H. Verder, C. Heiring, H. Clark, D. Sweet, T. E. Jessen, F. Ebbesen, L. J. Björklund, B. Andreasson, L. Bender, A. Bertelsen, M. Dahl, C. Eschen, J. Fenger-Grøn, S. F. Hoffmann, A. Höskuldsson, M. Bruusgaard-Mouritsen, F. Lundberg, A. D. Postle, P. Schousboe, P. Schmidt, H. Stanchev, L. Sørensen, *Acta Paediatr. Int. J Paediatr.* **2017**, *106*, 430.

[24] K. Czamara, K. Majzner, M. Z. Pacia, K. Kochan, A. Kaczor, M. Baranska, *J. Raman Spectrosc.* **2015**, *46*, 4.

[25] L. E. Jamieson, A. Li, K. Faulds, D. Graham, *R. Soc. Open Sci.* **2018**, *5*, 181483. https://doi.org/10.1098/rsos.181483

[26] K. Shirota, K. Yagi, T. Inaba, P. C. Li, M. Murata, Y. Sugita, T. Kobayashi, *Biophys. J.* **2016**, *111*, 999.

[27] C. B. Fox, R. H. Uibel, J. M. Harris, *J. Phys. Chem. B* **2007**, *111*, 11428.

[28] H. Akutsu, *Biochemistry* **1981**, *20*, 7359.

[29] K. G. Brown, E. Bicknell-Brown, M. Ladjadj, *J. Phys. Chem.* **1987**, *91*, 3436.

[30] R. N. Lewis, R. N. McElhaney, W. Pohle, H. H. Mantsch, *Biophys. J.* **1994**, *67*, 2367.

[31] C. Krafft, L. Neudert, T. Simat, R. Salzer, *Spectrochim. Acta - Part A Mol. Biomol. Spectrosc.* **2005**, *61*, 1529.

[32] P. Vandenabeele, J. Jehlička, P. Vítek, H. G. M. Edwards, *Planet. Space Sci.* **2012**, *62*, 48.

[33] T. R. Schlack, S. A. Beal, E. J. Corriveau, J. L. Clausen, *ACS Omega* **2021**, *6*, 16316.

[34] N. M. Ćulum, T. T. Cooper, G. I. Bell, D. A. Hess, F. Lagugné-Labarthet, *Anal. Bioanal. Chem.* **2021**, *413*, 5013.

[35] F. Menges, Spectragryph. https://www.effemm2.de/spectragryph/contact.html (Accessed 19 June 2023).

SUPPORTING INFORMATION

Additional supporting information can be found online in the Supporting Information section at the end of this article.

How to cite this article: A. V. Veluthandath, W. Ahmed, J. Madsen, H. W. Clark, A. D. Postle, J. S. Wilkinson, G. S. Murugan, *J Raman Spectrosc* **2023**, 1. https://doi.org/10.1002/jrs.6631